This article has been accepted for publication in a future issue of this journal, but has not been fully edited. Content may change prior to final publication. Citation information: DOI 10.1109/TPAMI.2015.2473839, IEEE Transactions on Pattern Analysis and Machine Intelligence

Separating Reflective and Fluorescent Components Using High Frequency Illumination in the Spectral Domain

Ying Fu, *Student Member, IEEE,* Antony Lam, *Member, IEEE*, Imari Sato, *Member, IEEE,* Takahiro Okabe, *Member, IEEE,* and Yoichi Sato, *Member, IEEE*

Abstract—Hyperspectral imaging is beneficial to many applications but most traditional methods do not consider fluorescent effects which are present in everyday items ranging from paper to even our food. Furthermore, everyday fluorescent items exhibit a mix of reflection and fluorescence so proper separation of these components is necessary for analyzing them. In recent years, effective imaging methods have been proposed but most require capturing the scene under multiple illuminants. In this paper, we demonstrate efficient separation and recovery of reflectance and fluorescence emission spectra through the use of two high frequency illuminations in the spectral domain. With the obtained fluorescence emission spectra from our high frequency illuminants, we then describe how to estimate the fluorescence absorption spectrum of a material given its emission spectrum. In addition, we provide an in depth analysis of our method and also show that filters can be used in conjunction with standard light sources to generate the required high frequency illuminants. We also test our method under ambient light and demonstrate an application of our method to synthetic relighting of real scenes.

Index Terms—Fluorescence absorption and emission spectra, reflectance spectra, high frequency illumination.

1 Introduction

Hyperspectral reflectance data are beneficial to many applications including but not limited to archiving for cultural e-heritage [1], medical imaging [2], and also color relighting of scenes [3]. As a result, many methods for acquiring the spectral reflectance of scenes have been proposed [4], [5], [6], [7], [8], [9]. Despite the success of these methods, they have all made the assumption that fluorescence is absent from the scene. However, fluorescence does frequently occur in many objects, such as natural gems and corals, fluorescent dyes used for clothing, and plant containing chlorophyll to name a few. In fact, Barnard shows that fluorescent surfaces are present in 20% of randomly constructed scenes [10]. This is a significant proportion of scenes that have not been considered by most of past methods.

Another important point is that reflective and fluorescent components behave very differently under different illuminants [3], [11]. Thus to accurately predict the color of objects, separate modeling of all spectral properties of both reflective and fluorescent components is essential. Specifically, when a reflective surface is illuminated by incident light, it reflects back light of the same wavelength. Fluorescent surfaces on the other hand, first absorb incident light and then emit at longer wavelengths. This wavelength shifting property is known as Stokes shift [12], [13] and the question of which wavelengths of light are absorbed and which wavelengths are emitted are defined by the fluorescent surface's absorption and emission spectra. As the properties of fluorescence are very different from ordinary reflection, neglecting fluorescence can result in completely incorrect color estimation. This in turn negatively affects many methods that rely on accurate color estimation. For example, algorithms for relighting and color constancy would be affected.

(a) White light (b) Reflection (c) Fluorescence

Fig. 1: (a) The scene captured under white light. (b) The recovered reflective component. (c)The recovered fluorescent component.

The goal of this paper is to accurately recover the full spectral reflective and fluorescent components of an entire scene. Typical fluorescent objects exhibit both reflection and fluorescence (Figure 1). So the question of how these components can be accurately separated also needs to be addressed. In this paper, we show that the

- *Y. Fu and Y. Sato are with Institute of Industrial Science, the University of Tokyo, Japan. E-mail: {fuying,ysato}@iis.u-tokyo.ac.jp*
- *A.Lam is with Saitama University, Japan. E-mail: antonylam@cv.ics.saitama-u.ac.jp*
- *I. Sato is with National Institute of Informatics, Japan. E-mail: imarik@nii.ac.jp*
- *T. Okabe is with Kyushu Institute of Technology, Japan. E-mail: okabe@ai.kyutech.ac.jp*

This article has been accepted for publication in a future issue of this journal, but has not been fully edited. Content may change prior to final publication. Citation information: DOI 10.1109/TPAMI.2015.2473839, IEEE Transactions on Pattern Analysis and Machine Intelligence

reflectance and fluorescence spectra of a scene can be efficiently separated and measured through the use of high frequency illumination in the spectral domain. Our approach only assumes that the absorption spectrum of the fluorescent material is a smooth function with respect to the frequency of the lighting in the spectral domain. With this assumption, it is possible to separate reflective and fluorescent components using just two hyperspectral images taken under a high frequency illumination pattern and its shifted version in the spectral domain. We show that the reflectance and fluorescence emission spectra can then be fully recovered by our separation method.

In addition to recovering reflectance and fluorescence emission spectra, we also make the observation that materials with similar emission spectra tend to have similar absorption spectra as well. Using this observation, we devise a method to estimate the absorption spectra by taking the corresponding recovered emission spectra from high frequency lighting.

In summary, our contributions are that we devise a method for efficient separation and recovery of full reflectance and fluorescence emission spectra, and present a method for estimating the absorption spectrum of a material given its emission. Since we completely recover the reflectance and fluorescence emission and absorption spectra of the scene, we also show our ability to accurately predict the relighting of scenes under novel lighting. In the preliminary version of this work [14], we employed an expensive programmable light source to produce high frequency illuminations used to separate and recover reflective-fluorescent spectral components of real scenes. In this paper, we provide a more in depth analysis of our method and also show that filters can be used in conjunction with standard light sources to generate the required high frequency illuminants. Thus bypassing the need for a programmable light source. We also extend our method to work under ambient light.

The rest of this paper is organized as follows. Section 2 reviews previous work in related areas. In Section 3, we describe the reflection and fluorescence models, and present our proposed high frequency spectra based separation method. In addition, we present our method's theoretical background and its error analysis. Section 4 presents our method for fluorescence absorption estimation. Section 5 provides experimental results on all estimated spectra, separated reflective and fluorescent components, and relighting results under a programmable light source. We also extend our method to more general light sources using two high frequency filters and show the use of our method under ambient light. Finally, conclusions are drawn and future directions of our research are discussed in Section 6.

2 Related Work

As noted earlier, there have been a number of papers on recovering the spectral reflectance of scenes [4], [5], [6], [7], [8], [9]. Despite the effectiveness of these methods for spectral reflectance capture, they do not take the effects of fluorescence into account.

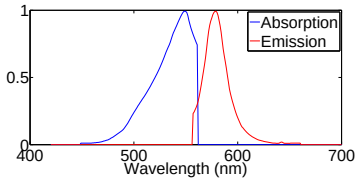

Fig. 2: An example of absorption and emission spectra from the McNamara and Boswell Fluorescence Spectral Dataset [15].

Unfortunately, not accounting for fluorescence can have a detrimental effect on color accuracy. For example, Johnson and Fairchild [3] showed that considering fluorescence can dramatically improve color renderings. Later, Wilkie *et al.* [16] showed accurate results by rendering fluorescence emissions using diffuse surfaces that can reflect light at a wavelength different from its incident illuminant wavelength. Hullin *et al.* [17] showed the importance of modeling and rendering of reflective-fluorescent materials using their bidirectional reflectance and reradiation distribution functions (BRRDF). Besides color rendering, the observation of fluorescence emissions on an object's surface has also been applied to photometric stereo for shape reconstruction [18], [19]. As mentioned earlier, Barnard concluded that fluorescent surfaces are present in 20% of randomly constructed scenes [10]. Thus the presence of fluorescence is significant and warrants attention.

In practice, fluorescent objects typically exhibit both reflection and fluorescence so the joint occurrence of these phenomena in scenes needs to be considered. Some methods in the literature have given this issue attention. Lee *et al.* [20] provided a mathematical description for fluorescence processes and recovered the additive spectra of reflective and fluorescent components but did not separate them. Alterman *et al.* [21] separated the appearance of fluorescent dyes from a mixture by unmixing multiplexed images. Zhang and Sato [11] derived an independent component analysis based method to estimate the RGB colors of reflectance and fluorescence emission but not their spectral distributions. They also did not estimate the absorption spectrum of the fluorescent component and so, cannot predict intensity changes in fluorescence emission due to different illumination spectra. Tominaga *et al.* [22] estimated fluorescence emission spectra using multispectral images taken under two ordinary light sources. A limitation is that they assumed fluorescence emissions to be constant for all absorption wavelengths and thus cannot accurately predict the brightness of fluorescent components under varying illumination. Finally, none of these methods fully recover all reflectance and fluorescence spectral components of scenes.

In recent work, methods for hyperspectral imaging of reflective-fluorescent scenes have been proposed. Lam and Sato [23] provided a method for recovering the full spectral reflectance and fluorescence absorption and

This article has been accepted for publication in a future issue of this journal, but has not been fully edited. Content may change prior to final publication. Citation information: DOI 10.1109/TPAMI.2015.2473839, IEEE Transactions on Pattern Analysis and Machine Intelligence

emission spectra of scenes but they needed to capture the scene about 30 times using a multiband camera under multiple narrowband illuminants. Suo *et al.* [24] presented a bispectral coding scheme which was rooted in the classical bispectral measurement method [25] where dozens of images also had to be captured under shifting narrowband illuminations. Zheng *et al.* [26] also recovered all the different types of fluorescence and reflectance spectra using off-the-shelf lights and three hyperspectral images. Fu *et al.* [27] recovered all these spectra by using an RGB camera and capturing under different illuminants. Both methods have advantages in that conventional light sources or cameras can be used but at the expense of accuracy. Our method only uses two hyperspectral images to recover all these spectra, and achieves highly accurate results with less illuminations.

As mentioned earlier, one of the key challenges in our problem is the separation of reflective and fluorescent components from composite objects exhibiting both phenomena. There have been a number of methods in the literature on separating components in images. For example, Farid and Adelson [28] used independent components analysis to separate reflections on glass and a painting on the side of the glass opposite the observer. Nayar *et al.* [29] separated specular reflections from diffuse reflections. It is interesting that an analogy can be made between our spectral domain work and the spatial domain work of Nayar *et al.* [30]. Whereas previous work [30] used high frequency spatial light patterns to separate lighting components in the spatial domain, we use high frequency light spectra to separate lighting components in the spectral domain.

3 Separation of Reflection and Fluorescence

In this section, we describe the reflection and fluorescence models used in our method, present the separation method for reflective and fluorescent components by using high frequency illumination, discuss the conditions required for the illumination frequencies, and analyze the errors of our method.

3.1 Reflection and Fluorescence Models

We begin with a brief review of how reflective-fluorescent materials are modeled [31]. Since reflection and fluorescence have different physical behaviors, they need to be described by different models.

The radiance of a reflective surface depends on incident light and its reflectance. The observed radiance of an ordinary reflective surface at wavelength λ is computed as

$$p_r(\lambda) = l(\lambda)r(\lambda), \tag{1}$$

where $l(\lambda)$ is the spectrum of the incident light at wavelength λ and $r(\lambda)$ is the spectral reflectance of the surface at wavelength λ.

The observed radiance of a pure fluorescent surface depends on the incident light, the material's absorption spectrum, and its emission spectrum. Fluorescence typically absorbs light at some wavelengths and emits them at longer wavelengths. The way this works is that when incident light hits a fluorescent surface, the surface's absorption spectrum will determine how much of the light is absorbed. Some of the absorbed energy is then released in the form of an emission spectrum at longer wavelengths than the incident light. The remainder of the absorbed energy is released as heat. The reason for this phenomenon is that fluorescence emission occurs after an orbital electron of a molecule, atom or nanostructure absorbs light and is excited, the electron relaxes to its ground state by emitting a photon of light and sends out heat after several nanoseconds. The shorter the light's wavelength is, the more energy the light carries. Since some of the absorbed energy is lost as heat, the fluorescence emission will be at a longer wavelength. Figure 2 illustrates an example of the absorption and emission spectra for a fluorescent material over the visible spectrum.

Let $l(\lambda')$ represent the intensity of the incident light at wavelength λ', the observed spectrum of a pure fluorescent surface [31] at wavelength λ is described as

$$p_f(\lambda) = \left(\int l(\lambda')a(\lambda')\mathrm{d}\lambda' \right) e(\lambda), \tag{2}$$

where $a(\lambda')$ and $e(\lambda)$ represent the absorption and emission spectrum, respectively. $\left(\int l(\lambda')a(\lambda')\mathrm{d}\lambda' \right)$ is determined by the absorption spectrum and the spectrum of the incoming light, and is independent of the emission spectrum. Replacing this part by scale factor k, Equation (2)[1] can be rewritten as $p_f(\lambda) = ke(\lambda)$, which means that the shape or the distribution of the emitted spectrum is constant, but the scale k of the emitted spectrum changes under different illuminations. In other words, the radiance of the fluorescence emission changes under different illuminations, but its color (specifically, chromaticity) stays the same regardless of illumination color.

The radiance of a reflective-fluorescent surface point can be expressed as a linear combination of the reflective component p_r and fluorescent component p_f, i.e. $p = p_r + p_f$. Thus,

$$p(\lambda) = l(\lambda)r(\lambda) + \left(\int l(\lambda')a(\lambda')\mathrm{d}\lambda' \right) e(\lambda). \tag{3}$$

3.2 Separation Using High Frequency Illumination

In our method, we use high frequency illumination defined in the spectral domain for separating reflective and fluorescent components. Let us start with simple binary

1. This model assumes that there is little overlap between the absorption and emission spectra. From our examination of fluorescent materials in the McNamara and Boswell fluorescence spectral dataset, overlap tends to be not so large. The average overlap is 50.66nm, and the average of intersection area between absorption and emission spectra is 14.47% of their area of union.

This article has been accepted for publication in a future issue of this journal, but has not been fully edited. Content may change prior to final publication. Citation information: DOI 10.1109/TPAMI.2015.2473839, IEEE Transactions on Pattern Analysis and Machine Intelligence

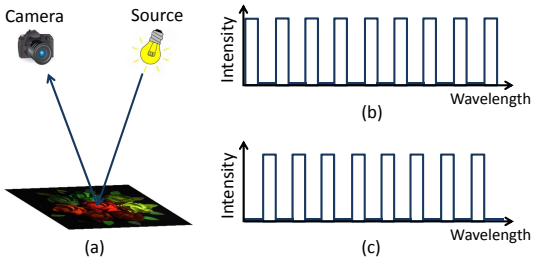

Fig. 3: An example of a captured scene (a). When a reflective-fluorescent point in the scene is lit by the illuminant (b), which is a high frequency binary illumination pattern in the wavelength domain, each lit wavelength includes both reflective and fluorescent components while the unlit wavelengths have only the fluorescent component. (c) shows its complement.

illuminants to describe the key idea of our method. We denote a high frequency illumination pattern shown in Figure 3(b) by $l_1(\lambda)$ and its complement shown in Figure 3(c) by $l_2(\lambda)$. The illuminants are defined such that when $l_1(\lambda)$ has intensity, $l_2(\lambda)$ has no intensity and vice versa. Let us consider a certain wavelength λ_1, where the wavelength λ_1 is lit directly under the illuminant $l_1(\lambda)$, so that $l_1(\lambda_1) = 1$ and then it is not lit under the illuminant l_2, so $l_2(\lambda_1) = 0$. Since reflection occurs at the same wavelength with the illumination, we obtain

$$\begin{aligned} p_1(\lambda_1) &= r(\lambda_1) + k'e(\lambda_1), \\ p_2(\lambda_1) &= k'e(\lambda_1). \end{aligned} \tag{4}$$

Here, we assume that $\int l_1(\lambda')a(\lambda')\mathrm{d}\lambda' = \int l_2(\lambda')a(\lambda')\mathrm{d}\lambda' = k'$. That is, the absorptions due to our high-frequency illumination patterns are the same. We will show in Section 3.3 this is true when the absorption $a(\lambda')$ is smooth with respect to the frequency of the illumination patterns in the spectral domain. With the same absorptions under the two illuminants, we obtain the reflectance and emission spectra at λ_1 as

$$\begin{aligned} r(\lambda_1) &= p_1(\lambda_1) - p_2(\lambda_1), \\ k'e(\lambda_1) &= p_2(\lambda_1). \end{aligned} \tag{5}$$

The reflectance and emission spectra at λ_2 where $l_1(\lambda_2) = 0$ and $l_2(\lambda_2) = 1$ are obtained in a similar manner.

In our work, we use high frequency sinusoidal illuminants (Figure 4) in the spectral domain to achieve the same effect as the binary lighting patterns because they are more practical and also fit into the theory of our framework. The illuminants can be represented as

$$\begin{aligned} l_1(\lambda) &= \alpha + \beta\cos(2\pi f_l\lambda), \\ l_2(\lambda) &= \alpha + \beta\cos(2\pi f_l\lambda + \phi). \end{aligned} \tag{6}$$

Where f_l is the frequency of illumination. The radiance of a surface under these two illuminants can be described as,

$$\begin{aligned} p_1(\lambda) &= l_1(\lambda)r(\lambda) + k_1e(\lambda), \\ p_2(\lambda) &= l_2(\lambda)r(\lambda) + k_2e(\lambda), \\ k_n &= \int l_n(\lambda')a(\lambda')\mathrm{d}\lambda'. \end{aligned} \tag{7}$$

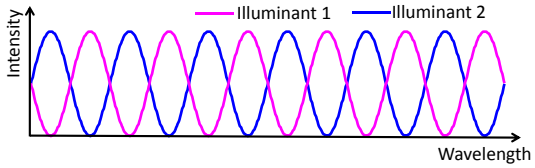

Fig. 4: Sinusoidal illuminant patterns. The blue and pink solid lines denote two illumination patterns. There is a phase shift between them.

Here, assuming that k_n is constant for l_1 and l_2, that is to say, $k_1 = k_2 = k$, the reflectance $r(\lambda)$ and fluorescence emission $ke(\lambda)$ can be recovered as

$$\begin{aligned} r(\lambda) &= \frac{p_1(\lambda) - p_2(\lambda)}{l_1(\lambda) - l_2(\lambda)}, \\ ke(\lambda) &= p_1(\lambda) - \frac{p_1(\lambda) - p_2(\lambda)}{l_1(\lambda) - l_2(\lambda)}l_1(\lambda). \end{aligned} \tag{8}$$

Thus, to recover the reflectance $r(\lambda)$ and fluorescence emission $ke(\lambda)$ completely, we first need to make $k_1 = k_2 = k$.

3.3 Discussion on the Illumination Frequency

In this section, we discuss how to satisfy the condition $k_1 = k_2 = k$. In the following, we consider the requirements for our illuminants based on the Nyquist sampling theorem [32] and on an analysis of the McNamara and Boswell fluorescence spectral dataset [15].

Let $a_n(\lambda) = l_n(\lambda)a(\lambda)$ $\{n = 1, 2\}$, where $l_n(\lambda)$ can be considered as a sampling or modulating function of $a(\lambda)$. The sampling theorem, which is most easily explained in terms of impulse-train sampling, establishes the fact that a band-limited signal is uniquely represented by its samples. In practice, however, narrow, large-amplitude pulses, which approximate impulses, are relatively difficult to generate and transmit. Instead, we use sinusoidal illuminant patterns in the spectral domain as shown in Figure 4. These patterns are similar to amplitude modulation functions in communication systems.

The spectrum of sinusoidal illumination $l_1(\lambda)$ in the frequency domain [32] is

$$L_1(f) = \frac{1}{2}[\beta\delta(f - f_l) + 2\alpha\delta(f) + \beta\delta(f + f_l)], \tag{9}$$

where $\delta(f)$ is the Dirac delta function. Let $A(f)$ and $A_n(f)$ denote the Fourier transform of $a(\lambda)$ and $a_n(\lambda)$, respectively. Since the product $l_n(\lambda)a(\lambda)$ in the spectral domain corresponds to a convolution in its Fourier domain, i.e.

$$A_n(f) = L_n(f) * A(f), \tag{10}$$

the Fourier transform of $a_1(\lambda)$ is

$$A_1(f) = \frac{1}{2}\left[\beta A(f - f_l) + 2\alpha A(f) + \beta A(f + f_l)\right]. \tag{11}$$

That is, a replication of the Fourier transform of the original signal $A(f)$ is centered around $+f_l$ and 0 and $-f_l$.

This article has been accepted for publication in a future issue of this journal, but has not been fully edited. Content may change prior to final publication. Citation information: DOI 10.1109/TPAMI.2015.2473839, IEEE Transactions on Pattern Analysis and Machine Intelligence

The Fourier transforms of $l_1(\lambda)$ and $l_2(\lambda)$ with the phase offset ϕ are related as $L_2(f) = e^{i\phi}L_1(f)$, and thus the frequency spectrum of $a_2(\lambda)$ is

$$A_2(f) = \frac{1}{2}[\beta e^{i\phi}A(f - f_l) + 2\alpha A(f) + \beta e^{-i\phi}A(f + f_l)]. \quad (12)$$

From the definition of the Fourier transform $A_n(f) = \int_{-\infty}^{+\infty} a_n(\lambda)e^{-i2\pi f\lambda}\mathrm{d}\lambda$, substituting $f = 0$ into this definition, we obtain

$$A_n(0) = \int_{-\infty}^{+\infty} a_n(\lambda)\mathrm{d}\lambda = \int_{-\infty}^{+\infty} l_n(\lambda)a(\lambda)\mathrm{d}\lambda = k_n. \quad (13)$$

Therefore, k_n corresponds to $A_n(f)$'s zero-frequency component. This tells us that we need to satisfy the condition $A_1(0) = A_2(0)$ so that $k_1 = k_2 = k$. In Equations (11) and (12), substituting $f = 0$, we obtain

$$A_1(0) = \frac{1}{2}\left[\beta A(-f_l) + 2\alpha A(0) + \beta A(f_l)\right], \quad A_2(0) = \frac{1}{2}[\beta e^{i\phi}A(-f_l) + 2\alpha A(0) + \beta e^{-i\phi}A(f_l)]. \quad (14)$$

Let us define f_a as $a(\lambda)$'s maximum frequency. When $f_l > f_a$, $A(-f_l)$ and $A(f_l)$ becomes zero. This means that we obtain $A_1(0) = A_2(0) = 2\alpha A(0)$ for $f_l > f_a$ to achieve $k_1 = k_2 = k$. Thus, the frequency of the illuminants in the spectral domain f_l needs to be greater than $a(\lambda)$'s maximum frequency or bandwidth f_a.

We now discuss the maximum frequency of $a(\lambda)$ on the McNamara and Boswell fluorescence spectral dataset. We examine the maximum frequency of all 509 materials in the dataset, and obtain the maximum frequency of each absorption spectrum while retaining 99% of the energy[1]. The mean of the maximum frequency for all absorption spectra in the dataset is $1/45.9[nm^{-1}]$ and its standard deviation is $1/24.1[nm^{-1}]$. As mentioned previously, the illumination frequency f_l needs to be greater than $a(\lambda)$'s maximum frequency f_a. As the period is the reciprocal of the frequency, the period of the illumination – which we call the "sampling interval" – in the spectral domain needs to be less than the minimum sampling interval of all absorption spectra of fluorescent materials in the scene. Figure 5 shows the percentage of absorption spectra in the McNamara and Boswell fluorescence spectral dataset that satisfy the condition $k_1 = k_2$ under different periods of the illumination. We set the period of the illumination to 40 nm in our experiments due to limitations of our light source. This is still less than the mean minimum sampling interval of all absorption spectra (45.9 nm) found in the dataset and works well in practice.

3.4 Error Analysis

Due to limitations of the light source, we cannot produce ideal and arbitrary high frequency illuminations. It is thus unlikely for k to be the exact constant for all kinds of fluorescent materials in the scene under realistic conditions. Therefore, to reduce errors, we substitute the recovered $r(\lambda)$ into both $p_1(\lambda) = l_1(\lambda)r(\lambda) + k_1e(\lambda)$ and $p_2(\lambda) = l_2(\lambda)r(\lambda) + k_2e(\lambda)$, and average the recovered $ke(\lambda)$ from these two equations. Thus, the fluorescence emission $ke(\lambda)$ is recovered by

$$\begin{aligned} ke(\lambda) =& \frac{1}{2}\left[k_1e(\lambda) + k_2e(\lambda)\right] \\ =& \frac{1}{2}\Big[p_1(\lambda) - \frac{p_1(\lambda) - p_2(\lambda)}{l_1(\lambda) - l_2(\lambda)}l_1(\lambda) + \\ & p_2(\lambda) - \frac{p_1(\lambda) - p_2(\lambda)}{l_1(\lambda) - l_2(\lambda)}l_2(\lambda)\Big]. \end{aligned} \quad (15)$$

If $k_1 \neq k_2$,

$$r(\lambda) = \frac{(p_1(\lambda) - p_2(\lambda)) - (k_1 - k_2)e(\lambda)}{l_1(\lambda) - l_2(\lambda)}. \quad (16)$$

Let $r_{error}(\lambda)$ and $e_{error}(\lambda)$ denote the errors of $r(\lambda)$ and $ke(\lambda)$ (where $k = (k_1 + k_2)/2$ when $k_1 \neq k_2$). These errors can be expressed as

$$r_{error}(\lambda) = abs\left[\frac{(k_1 - k_2)e(\lambda)}{l_1(\lambda) - l_2(\lambda)}\right], \quad e_{error}(\lambda) = abs\left[(k_1 - k_2)e(\lambda)\frac{l_1(\lambda) + l_2(\lambda)}{2\left[l_1(\lambda) - l_2(\lambda)\right]}\right]. \quad (17)$$

For the sinusoidal illuminant $l_n(\lambda)$ in Equation (6), the maximum and minimum intensities over all wavelengths λ are $\alpha + \beta$ and $\alpha - \beta$. Each value in an illuminant's spectrum has to be positive, so $\alpha/\beta \geq 1$.

In Equation (17), the errors for the reflective and fluorescence emission are directly proportional to $k_1 - k_2$. This means that the less difference between k_1 and k_2 there is, the smaller the errors. As α/β becomes larger, $A_1(0)$ and $A_2(0)$ in Equation (14) are less affected by the $\beta A(-f_l)$ and $\beta A(f_l)$ terms. As a result, the difference between k_1 and k_2 can be decreased under the same illumination frequency. Thus the k term is more robust under different illumination conditions, when α/β is large.

Nevertheless, when the scene is captured by the camera, the noise from the camera cannot be totally avoided. As $l_1(\lambda) - l_2(\lambda)$ shrinks, $r(\lambda)$ and $e(\lambda)$ are increasingly affected by noise, as can be seen in Equation (8). In order to make the proposed method more robust to noise, we need to make the difference $l_1(\lambda) - l_2(\lambda)$ greater.

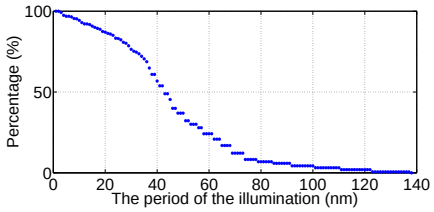

Fig. 5: The percentage of absorption spectra in the McNamara and Boswell fluorescence spectral dataset where $k_1 = k_2$ given different the period of the illumination. The smaller the period of the illumination, the more absorption spectra satisfy our requirement that $k_1 = k_2$.

1. Since there exists some noise in the original spectra, ignoring some high frequency components is reasonable.

This article has been accepted for publication in a future issue of this journal, but has not been fully edited. Content may change prior to final publication. Citation information: DOI 10.1109/TPAMI.2015.2473839, IEEE Transactions on Pattern Analysis and Machine Intelligence

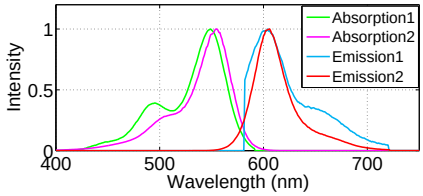

Fig. 6: Absorption and emission spectra of two fluorescent materials.

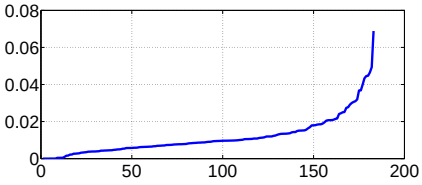

Fig. 7: All test errors sorted in ascending order. 67% of cases were below the average error of 0.012.

In practice, we set the phase shift of illuminations $l_1(\lambda)$ and $l_2(\lambda)$ to π (Figure 4) and capture the scene at the illumination's peaks or crests to maximize the observed difference in $l_1(\lambda) - l_2(\lambda)$.

It is also interesting to note that the need to maximize $l_1(\lambda) - l_2(\lambda)$ also means that α/β should be closer to 1, which is at odds with the need to make α/β large to allow for a more robust k as discussed above. We will discuss the influence and tradeoffs of the value of α/β in real data in Sections 5.4 and 5.5.

4 Estimating the Absorption Spectra

In this section, we will explain how we estimate the absorption spectrum of a material from its emission spectrum that was obtained using our method in Section 3.2.

The basic observation behind our method is that fluorescent materials with similar emission spectra tend to have similar absorption spectra (Figure 6). From this observation, we derive a method that uses a dictionary of known emission and absorption spectrum pairs to estimate an absorption spectrum from a given novel emission.

Specifically, let $\hat{\boldsymbol{e}}$ be a known emission spectrum whose absorption spectrum $\hat{\boldsymbol{a}}$ is unknown. Let $\{\boldsymbol{e}_j\}$ be a dictionary of emission spectra and $\{\boldsymbol{a}_j\}$ be the known corresponding absorption spectra. Representing all these spectra as vectors, we first determine the linear combination of $\{\boldsymbol{e}_j\}$ to reconstruct $\hat{\boldsymbol{e}}$ by solving

$$\hat{\boldsymbol{e}} = \sum\nolimits_j w_j \boldsymbol{e}_j. \tag{18}$$

The weights $\{w_j\}$ are then used to calculate the corresponding absorption spectrum $\hat{\boldsymbol{a}}$ by

$$\hat{\boldsymbol{a}} = \sum\nolimits_j w_j \boldsymbol{a}_j. \tag{19}$$

Let $\{\boldsymbol{e}_j^{'}\}$ and $\{\boldsymbol{a}_j^{'}\}$ denote the subsets of $\{\boldsymbol{e}_j\}$ and $\{\boldsymbol{a}_j\}$ whose corresponding weights $\{w_j \neq 0\}$. Note that using the same $\{w_j\}$ in Equation (18) and (19) requires the linear combination be kept between the subspaces spanned by $\{\boldsymbol{e}_j^{'}\}$ and $\{\boldsymbol{a}_j^{'}\}$. We assert that an emission spectrum can typically be well-represented by a sparse basis. To show this, we perform leave-one-out cross-validation where for each emission spectrum in the McNamara and Boswell fluorescence spectral dataset, we set $\hat{\boldsymbol{e}}$ as the testing sample and use the remaining emission spectra in $\{\boldsymbol{e}_j\}$ as the dictionary. We find that any given emission $\hat{\boldsymbol{e}}$ can on average be well represented by 10 emission spectra from the dictionary, which is very sparse compared to the size of the whole dictionary. Thus $\hat{\boldsymbol{e}}$ can considered to live in a low-dimensional sub-space spanned by $\{\boldsymbol{e}_j^{'}\}$. Therefore, to minimize the number of basis vectors used from $\{\boldsymbol{e}_j\}$, we seek to reconstruct $\hat{\boldsymbol{e}}$ by sparse weights $\boldsymbol{w}$ through l_1-norm minimization [33], [34], [35], according to

$$\min \|\boldsymbol{w}\|_1 \quad s.t. \quad w_j \geq 0 \text{ and } \left\|\hat{\boldsymbol{e}} - \sum\nolimits_j w_j \boldsymbol{e}_j\right\|_2^2 \leq \epsilon. \tag{20}$$

To test the accuracy of our method, we chose a subset of materials from the McNamara and Boswell fluorescence spectral dataset where both the emission and absorption spectra are present in the visible range (400 -

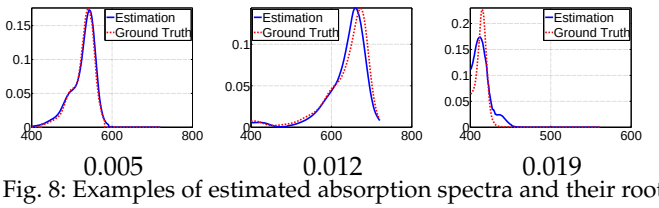

Fig. 8: Examples of estimated absorption spectra and their root-mean-square-errors.

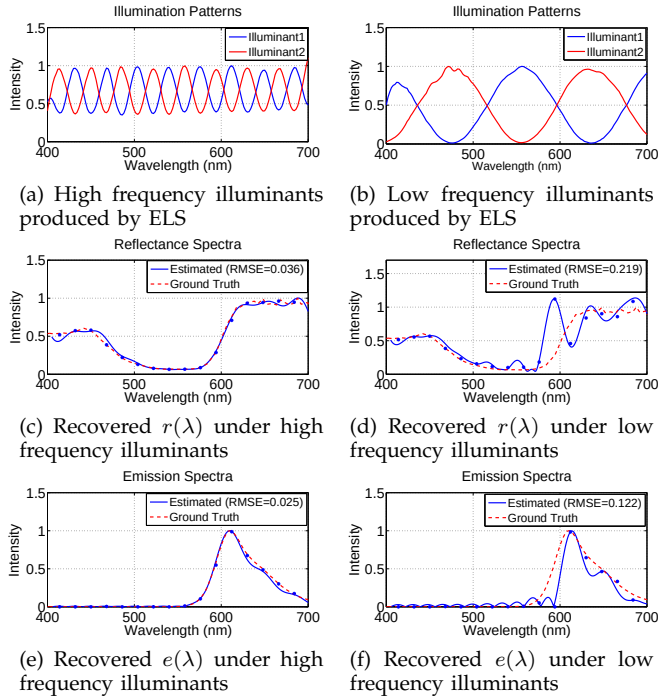

(a) High frequency illuminants produced by ELS

(b) Low frequency illuminants produced by ELS

(c) Recovered $r(\lambda)$ under high frequency illuminants

(d) Recovered $r(\lambda)$ under low frequency illuminants

(e) Recovered $e(\lambda)$ under high frequency illuminants

(f) Recovered $e(\lambda)$ under low frequency illuminants

Fig. 9: Evaluation of our separation method on a pink sheet (■). (a) Two high frequency illuminations. (c) and (e) show the recovered reflectance and fluorescence emission spectra under these high frequency illuminations, respectively. (b) Two low frequency illuminations. (d) and (f) show the recovered reflectance and fluorescence emission spectra under these low frequency illuminations, respectively. The red lines show the ground truths and the blue lines show the estimated results.

This article has been accepted for publication in a future issue of this journal, but has not been fully edited. Content may change prior to final publication. Citation information: DOI 10.1109/TPAMI.2015.2473839, IEEE Transactions on Pattern Analysis and Machine Intelligence

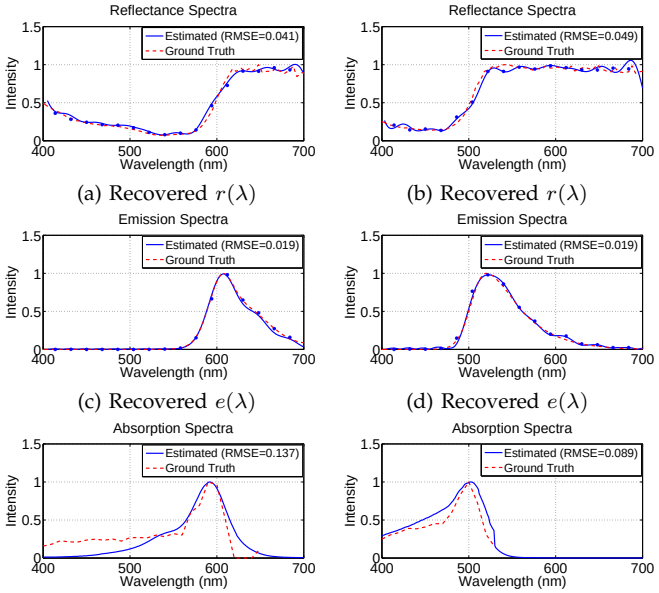

(a) Recovered $r(\lambda)$ (b) Recovered $r(\lambda)$

(c) Recovered $e(\lambda)$ (d) Recovered $e(\lambda)$

(e) Recovered $a(\lambda)$ (f) Recovered $a(\lambda)$

Fig. 10: Recovered reflectance $r(\lambda)$, fluorescence emission $e(\lambda)$ and absorption $a(\lambda)$ spectra of the red (■) and yellow (■) sheets.

720 nm). This results in a collection of 183 materials. We then perform leave-one-out cross-validation using our method and the 183 emission and absorption spectra. The estimated absorption spectrum is then compared against the ground truth using the mean root square error $\sqrt{\left(\sum_\lambda \left(a^{gt}(\lambda) - a^{re}(\lambda)\right)^2 d\lambda\right)}/N$, where $a^{gt}(\lambda)$ and $a^{re}(\lambda)$ are the ground truth and recovered spectra at wavelength λ, respectively. N is the discrete number of wavelengths representing the spectrum in the visible range. The ground truth and estimation are also normalized for scale by setting them to be unit length vectors.

In our results, we obtain an average error of 0.012. See Figure 7 for a plot of all the errors for the 183 estimated absorption spectra. We do find a minority of cases with high errors that violate our assumption that similar emission spectra map to the same absorption spectra. Despite this, the majority of materials fit our assumption and absorption spectra are accurately estimated as seen in Figure 8. We also note that absorption only determines the scale of the emission and not the color of the material. Thus some minor loss in accuracy for estimated absorption does not have a dramatic effect on the predicted color of scenes.

5 Experiment Results and Analysis

In our experiments, we first demonstrate the importance of high frequency illumination using quantitative results on the recovery of reflectance and fluorescence spectra from real scenes. We then present visual examples of separated reflective and fluorescent components using images captured under high frequency illuminations produced by a programmable light source, and use our recovered spectra to accurately relight fluorescent scenes.

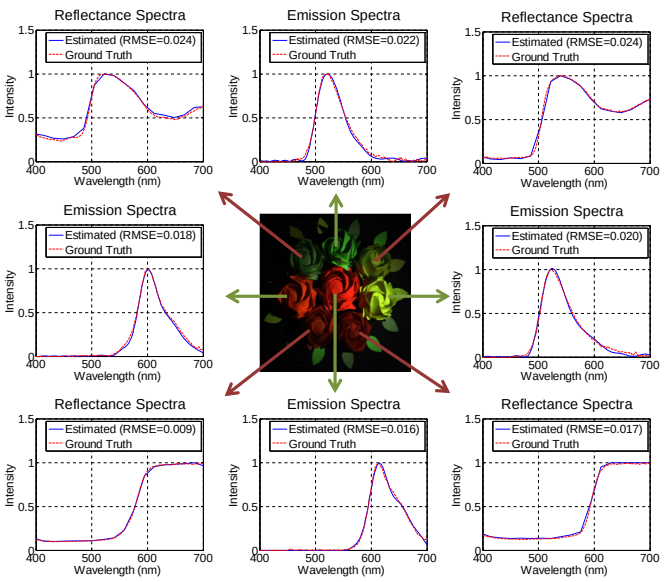

Fig. 11: Recovered reflectance spectra for the ordinary reflective materials (red arrows) and fluorescence emission spectra for the fluorescent materials (green arrows).

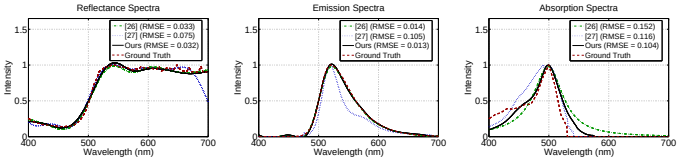

(a) Recovered $r(\lambda)$ (b) Recovered $e(\lambda)$ (c) Recovered $a(\lambda)$

Fig. 12: Comparison results on the fluorescent yellow sheet.

We then bypass the need for an expensive programmable light source by using filters in conjunction with standard light sources to generate the required high frequency illuminants. Finally, we show that our method also works under ambient light.

5.1 Experimental Setup

With the exception of near UV light and ambient lights used in Subsection 5.5, for all other illuminants in this section, we use a Nikon Equalized Light Source (ELS). The ELS is a programmable light source that can produce light with arbitrary spectral patterns from 400 nm to 720 nm. We use a PR-670 SpectraScan Spectroradiometer to collect ground truth spectra. For our proposed method, we use a hyperspectral camera (EBA Japan NH-7) to capture whole scenes.

Figure 9(a) shows two high frequency illuminants produced by the ELS. Under these illuminants, we use the hyperspectral camera to capture the scene at wavelengths where either one of these illuminants have peaks so that the difference between l_1 and l_2 would be large and allow for reliable separation.

5.2 Quantitative Evaluation of Recovered Spectra

In this section, we first compare quantitative results on recovering the reflectance and fluorescence spectral components using high and low frequency lights on

This article has been accepted for publication in a future issue of this journal, but has not been fully edited. Content may change prior to final publication. Citation information: DOI 10.1109/TPAMI.2015.2473839, IEEE Transactions on Pattern Analysis and Machine Intelligence

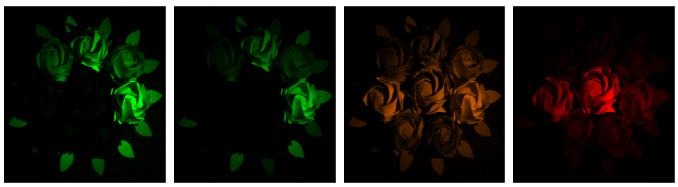

(a) Four captured channels under illuminant l_1

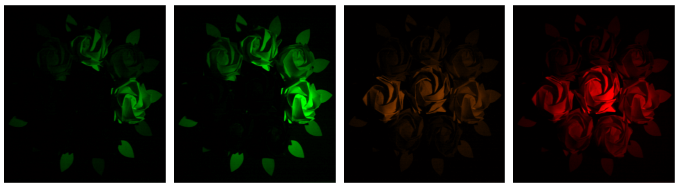

(b) Four captured channels under illuminant l_2

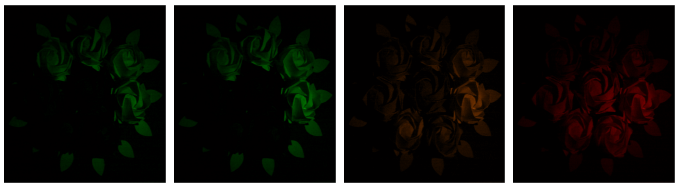

(c) Separated reflective components on 4 channels

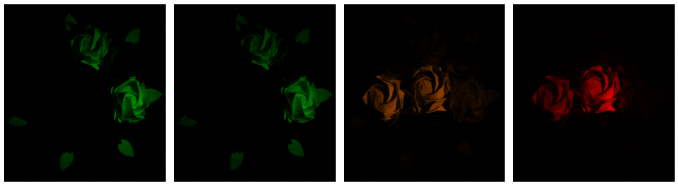

(d) Separated fluorescent components on 4 channels

Fig. 13: The separation results on 4 channels of the hyperspectral images for a scene with fluorescent and non-fluorescent roses. These four channels, from left to right, are at 520 nm, 540 nm, 600 nm, and 620 nm.

(a) Illuminant l_1 (b) Illuminant l_2 (c) Near UV light

(d) Green light (e) Relighted (f) Relighted (Ref)

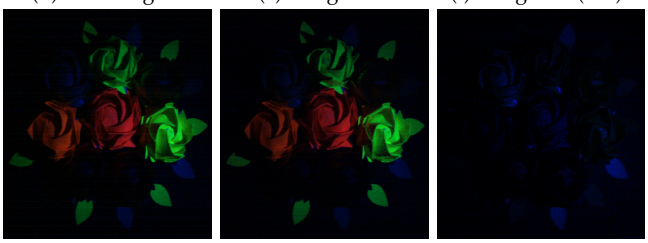

(g) Blue light (h) Relighted (i) Relighted (Ref)

Fig. 14: The relighting results for a scene with fluorescent and non-fluorescent roses. "Ref" denotes relighting with only the reflective component.

fluorescent colored sheets. To make the quantitative evaluation, we measure the root mean square error (RMSE) of the estimated spectra, with respect to their corresponding ground truth. Figure 9(a) and (c) show spectral distributions of the high frequency and low frequency illuminants used in our experiments. These illuminants are then used to recover spectra that are compared against the ground truth spectra.

The ground truth reflectance and fluorescent absorption and emission spectra of the fluorescent material are captured by bispectral measurements [25]. In this procedure, narrowband illuminants are employed across the visible spectrum. The reflectance spectra are measured at the same wavelength as the narrowband illuminant, fluorescence emission spectra are measured at longer wavelengths than the illuminations, and fluorescence absorption spectra are measured by observing the emission at a certain wavelength λ while varying the illuminant wavelength $\lambda^{'}$ for $\lambda^{'} < \lambda$.

In Figure 9(b)-(f), we see the recovered reflectance and fluorescence emission spectra of a pink fluorescent sheet under different frequency illuminants. The recovered reflectance (Figure 9(b)) and fluorescence emission spectra (Figure 9(e)) under the high frequency illuminants approximate the ground truth well. When the object is captured under the low frequency illuminants, the recovered reflectance (Figure 9(d)) and fluorescence emission (Figure 9(f)) have obvious errors. Figure 10(a)-(d) shows the recovered reflectance and fluorescence emission spectra of the red and yellow fluorescent sheets under the high frequency illuminants. All these results demonstrate that our method is able to recover reflectance and fluorescence emission spectra efficiently under high frequency illuminants.

In Figure 10(e) and (f), the recovered fluorescence absorption spectra of the red and yellow fluorescent sheets are shown. Due to limitations of our capture equipment, the ground truth could not be accurately measured in the short wavelength region in cases where absorption was relatively weak. This issue can be seen in the shorter wavelengths for the red sheet (Figure 10(e)). However, we can see that the recovered absorption spectra and the ground truth measurements still agree quite well.

We now show that our method works well for both ordinary reflective materials and fluoresent materials. For ordinary reflective materials, the reflectance spectrum can be easily recovered by capturing the scene under white light across the visible spectrum, while the emission spectrum for a fluorescent material can be easily captured at longer wavelengths under near UV light. Generally, a scene consists of both ordinary reflective materials and fluorescent materials. Here, we first evaluate the recovered reflectance spectra for ordinary reflective materials and the emission spectra for fluorescent materials. Their ground truth data are captured

This article has been accepted for publication in a future issue of this journal, but has not been fully edited. Content may change prior to final publication. Citation information: DOI 10.1109/TPAMI.2015.2473839, IEEE Transactions on Pattern Analysis and Machine Intelligence

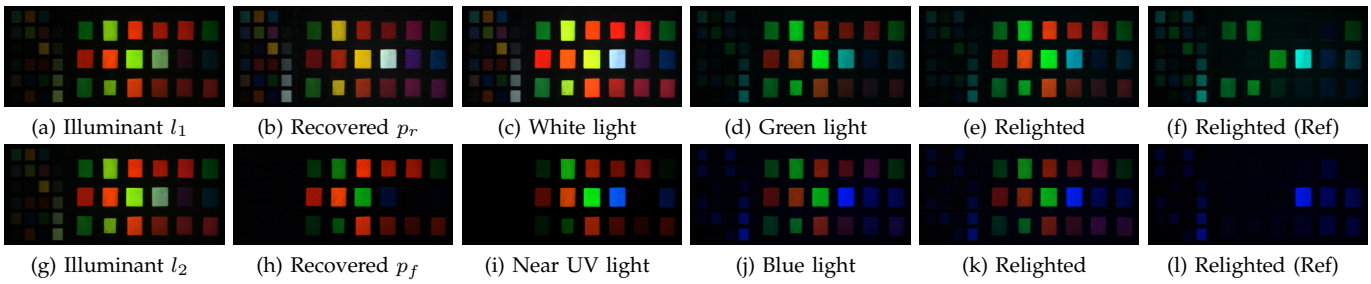

(a) Illuminant l_1 (b) Recovered p_r (c) White light (d) Green light (e) Relighted (f) Relighted (Ref)

(g) Illuminant l_2 (h) Recovered p_f (i) Near UV light (j) Blue light (k) Relighted (l) Relighted (Ref)

Fig. 15: Separation and relighting results for a fluorescent and a non-fluorescent color chart.

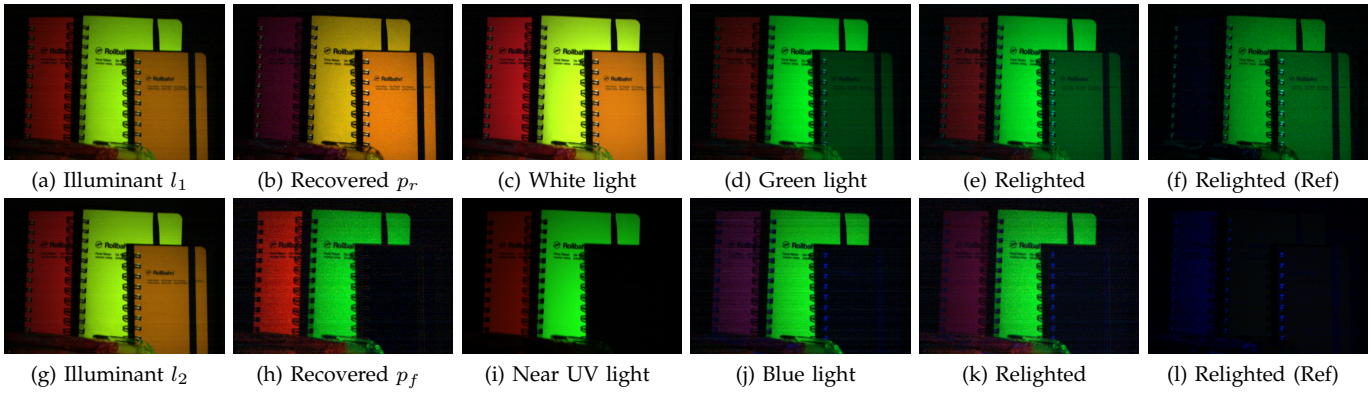

(a) Illuminant l_1 (b) Recovered p_r (c) White light (d) Green light (e) Relighted (f) Relighted (Ref)

(g) Illuminant l_2 (h) Recovered p_f (i) Near UV light (j) Blue light (k) Relighted (l) Relighted (Ref)

Fig. 16: Separation and relighting results for a scene with fluorescent and non-fluorescent objects.

under white light and near UV light, respectively. In our method, the reflectance spectrum $r(\lambda)$ and the emission spectrum $e(\lambda)$ are estimated by Equations (8) at the same time. Figure 11 shows recovered reflectance spectra for ordinary materials (red arrows) and fluorescence emission spectra for the fluorescent materials (green arrows) by using high frequency illuminations. We can see that all recovered spectra (blue line) approximate the ground truth (red line) well. This demonstrates that our method can effectively separate fluorescent emission spectra $e(\lambda)$ from the fluorescent material, and also works for ordinary reflective materials, in which $e(\lambda) = 0$, $r(\lambda)$ can be well recovered by the first Equation in (8).

We also compared our method against state-of-art works [26] [27]. To allow for the fairest comparison under ideal conditions with all these methods, we performed synthetic tests. As shown in Figure 12, we can see that our method achieves similar accuracy to [26], which uses three hyperspectral images and needs to capture enough hyperspectral bands to separate reflective and fluorescent components, while our method uses two hyperspectral images and can also separate reflective and fluorescent components for any number of narrowband channels under these two high frequency light spectra. Compared against [27], which uses multiple color RGB images, we achieve high accuracy results.

5.3 Visual Separation and Relighting Results

In this section, we show results for the separation of reflection and fluorescence as well as accurate relighting performance on visual images. Our original results are in the form of hyperspectral images. Figure 13 shows four channels of the hyperspectral images and separated results by using high frequency illuminations for a fluorescent scene. From the left to the right columns, Figure 13(a) shows the scene captured at the peak, crest, peak, and crest wavelengths of illuminant l_1. Correspondingly Figure 13(b) shows the scene captured at the crest, peak, crest, and peak of illuminant l_2 at the same wavelengths. The wavelengths get longer from the left to right columns. Their separated reflective and fluorescent components are shown in Figure 13(c) and (d), respectively. The separated fluorescent components (Figure 13(d)) only contain the fluorescent material, and demonstrate that our method can effectively separate the reflective and fluorescent components. We also see that the green and yellow fluorescent roses are clearly visible in the shorter wavelengths (the first and second columns in Figure 13(d)) and the orange and red fluorescent roses are clearly visible in the longer wavelengths (the third and fourth columns in Figure 13(d)).

To easily visualize hyperspectral images, we have converted them all to RGB images in the following. The first scene is an image consisting of fluorescent and non-fluorescent roses and is taken under two high frequency illuminants (Figure 14(a) and (b)). Figure 1(b) and (c) are the corresponding separated reflective and fluorescent components. The roses in 4 corners (the red arrows in Figure 11) only have ordinary reflection so their colors in the recovered reflective component (Figure 1(b)) are the same as those seen under white light (Figure 1(a)). Looking at the center rose, which is made from the red sheet in Figure 1(a), we see that the recovered fluorescent component appears to be red. The measured emission spectrum of the red sheet (Figure 10(c)) indicates that

This article has been accepted for publication in a future issue of this journal, but has not been fully edited. Content may change prior to final publication. Citation information: DOI 10.1109/TPAMI.2015.2473839, IEEE Transactions on Pattern Analysis and Machine Intelligence

the color of the fluorescent component is indeed red. In addition, the scene captured under near UV light (Figure 14(c)) shows nearly pure fluorescent emission colors that also agree with our results in Figure 1(c). We note that since each fluorescent material has its own absorption spectrum, the value for $\left(\int l(\lambda^{'})a(\lambda^{'})\mathrm{d}\lambda^{'}\right)$ is different between fluorescent materials captured under near UV light and high frequency light. As a result, under different lighting, fluorescent objects can exhibit different scales of emission, but the chromaticities match well as can be seen by comparing the images under near UV light (Figure 14(c)) and for the recovered fluorescent component (Figure 1(c)).

Since our method is able to recover the full reflectance, fluorescence emission, and fluorescence absorption spectra for an entire scene, we are also able to relight scenes. Figure 14 shows that real scenes can be accurately relighted using our method. The scenes are captured under green (Figure 14(d)) and blue (Figure 14(g)) illuminants. The corresponding relighting results are shown in Figure 14(e) and (h). We can see that, the relighting results are very similar to the ground truths (Figure 14(d) and (g)), and demonstrate the effectiveness of our method in recovering the reflectance and fluorescence emission and absorption spectra. When the scene is relighted using the reflective component only (Figure 14(f) and (i)), this leads to many fluorescent materials appearing as black, especially under blue light (Figure 14(i)).

Figures 15 and 16 show additional separation of reflection and fluorescence on two other fluorescent scenes and their relighting results. They are a fluorescent color checker with a Macbeth color chart, and fluorescent and non-fluorescent notebooks. The separated reflective component (Figure 15-16(b)) for the ordinary reflective material is the same as those seen under white light (Figure 15-16(c)), and the separated fluorescent component (Figure 15-16(h)) also approximates the scene captured under near UV light (Figure 15-16(i)) which shows nearly pure fluorescence emission colors. The relighting results (Figure 15-16(e)(k)) were all close to the ground truth (Figure 15-16(d)(j)). These additional results on real scenes show that our method is effective for different scenes.

5.4 Separation by Using High Frequency Filters

In the previous parts of this section, we employ a programmable light source known as the ELS to produce complementary high frequency illuminants, by which the excellent experimental results can be obtained. However, programmable light sources such as the ELS are prohibitively expensive for many laboratories and consumers. They are also heavy and thus not portable. Due to these limitations, we designed two complementary high frequency filters, which are portable, as shown in Figure 17. These two filters are put in front of a light source to modulate an illuminant into high frequency illuminations that are the same as the lights produced

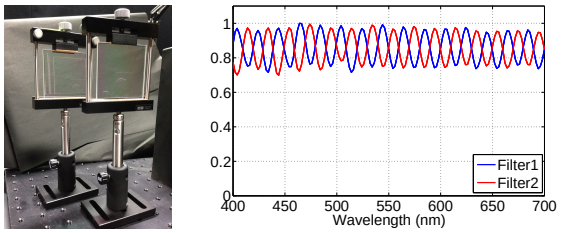

(a) Filters (b) Spectra

Fig. 17: The two high frequency filters (a) and their spectra (b).

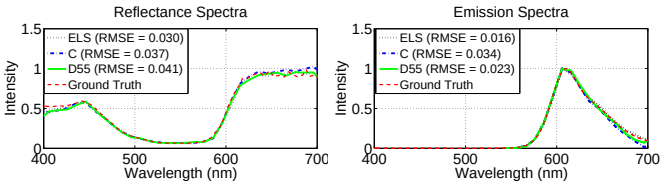

(a) Recovered $r(\lambda)$ (b) Recovered $e(\lambda)$

Fig. 18: Recovered reflectance $r(\lambda)$ and fluorescence emission $e(\lambda)$ of a pink fluorescent sheet under high frequency illuminants produced by the ELS, and C light through high frequency filters and D55 light through high frequency filters.

by the programmable light source. They are designed as two complementary sinusoidal patterns with periods of 20 nm [2].

Let us denote one of filters as F_1 and its complement as F_2. The illumination $l(\lambda)$ after going through the filters can be described as

$$\begin{aligned} l_1^f(\lambda) &= F_1(\lambda)l(\lambda), \\ l_2^f(\lambda) &= F_2(\lambda)l(\lambda). \end{aligned} \tag{21}$$

When the spectrum of light $l(\lambda)$ is flat (constant for all wavelengths λ), we can see that l_n^f $(n = 1, 2)$ are equivalent to the lights l_n $(n = 1, 2)$ discussed in Section 3.

However, common light sources such as daylight and off-the-shelf lights are not exactly flat, so we need to evaluate how an arbitrary light source affects the resultant high frequency illuminations. We first replace $l_n(\lambda)$ with $l_n^f(\lambda)$ in Equation (7) and obtain

$$\begin{aligned} p_1(\lambda) &= F_1(\lambda)l(\lambda)r(\lambda) + k_1 e(\lambda), \\ p_2(\lambda) &= F_2(\lambda)l(\lambda)r(\lambda) + k_2 e(\lambda), \\ k_n &= \int F_n(\lambda^{'})l(\lambda^{'})a(\lambda^{'})\mathrm{d}\lambda^{'}. \end{aligned} \tag{22}$$

As discussed in Section 3.4, the errors for the recovered reflectance and fluorescence emission spectra are directly proportional to $k_1 - k_2$. In this case, the difference between k_1 and k_2 is decided by the spectra of the filters $F_n(\lambda)$, illuminant $l(\lambda)$ and fluorescent absorption $a(\lambda)$. Table 1 shows the mean percent differences between k_1 and k_2 for 183 absorption spectra, where each row corresponds to a CIE standard illuminant. To explore the influences due to the frequency and the appearance of the filters, we calculate the mean percentage on 3 kinds

2. Due to limitations in manufacturing of the filters, we cannot produce the exact sinusoidal spectra in the filters.

This article has been accepted for publication in a future issue of this journal, but has not been fully edited. Content may change prior to final publication. Citation information: DOI 10.1109/TPAMI.2015.2473839, IEEE Transactions on Pattern Analysis and Machine Intelligence

TABLE 1: The mean percent difference between k_1 and k_2 for 183 absorption spectra on CIE Standard Illuminants [36] with the ideal sinusoidal pattern filters and real filters. "Ideal (20 nm)" and "Ideal (40 nm)" denote filters with ideal sinusoidal patterns and periods of 20 nm and 40 nm. "Real Filters" are the filters used in our experiments and their spectra are shown in Figure 17.

Illuminant	Ideal (40 nm)	Ideal (20 nm)	Real Filters
E	2.56	0.34	0.44
A	2.79	0.33	0.37
B	2.64	0.29	0.36
C	2.59	0.28	0.36
D50	2.70	0.46	0.42
D55	2.66	0.45	0.42
D65	2.61	0.44	0.43
D75	2.57	0.43	0.44
F1	8.06	1.41	0.44
F2	9.57	1.74	0.59
F3	11.25	2.13	0.77
F4	13.00	2.56	0.97
F5	7.92	1.36	0.41
F6	9.92	1.80	0.62
F7	7.82	1.33	0.43
F8	8.74	1.50	0.54
F9	9.86	1.74	0.65
F10	14.56	3.12	1.02
F11	16.58	3.73	1.21
F12	19.20	4.52	1.47

of filters, "Ideal (40 nm)", "Ideal (20 nm)", and "Real Filters".

"Ideal (40 nm)" and "Ideal (20 nm)" denote ideal sinusoidal patterned filters with 40 nm and 20 nm periods and ratio $\alpha/\beta = 1$. According to the discussion in Section 3.3, when the frequency of the filters is higher, the difference between k_1 and k_2 will be lower. In Table 1, we can see that the differences under "Ideal (20 nm)" are less than those under "Ideal (40 nm)" under the same illuminant $l(\lambda)$.

The real filters shown in Figure 17 approximate the ideal sinusoidal patterns well and have the same period as the "Ideal (20 nm)" filters, but the value, α/β of the real filters is larger. Recall that in Section 3.4, we discussed that the difference between k_1 and k_2 relies on the high frequency component $\beta\cos(2\pi f_l\lambda)$ in the illuminant and is not related to the direct current (DC) component α. Thus, when the ratio α/β becomes larger, the difference between k_1 and k_2 is reduced. As shown in Table 1, under most standard illuminants, the difference between k_1 and k_2 under "Real Filters" is lower than for the "Ideal (20 nm)" filters for the same standard illuminant. Nevertheless, in some cases, the difference between k_1 and k_2 under "Real Filters" is a little larger than those in the "Ideal (20 nm)" filters. This is because the real filters are not the exact sinusoidal spectra and exhibit some distortions. Figure 18 shows the recovered reflectance $r(\lambda)$ and fluorescence emission $e(\lambda)$ of a pink fluorescent sheet under high frequency illuminants produced by the ELS, C light through high frequency filters, and D55 light through high frequency filters. All these recovered spectra approximate the ground truth well. This indicates that the errors for recovered reflectance and emission spectra are acceptable and our method is effective using high frequency filters on real data.

Figure 19 shows the separated reflective and fluorescent components under different illuminants through the high frequency filters. The first column shows the high frequency illuminations' spectra, resulting from using different light sources. Taking a channel at 550 nm as an example, the second and third columns show the captured images under two high frequency illuminations, and their separation results are shown in the third and fourth columns. The fifth and sixth columns show separation results over all captured spectra in RGB images. Figure 19(b)-(d) show the separation results under C, D55 and F5 lights with the high frequency filters, respectively. Compared with the separation results under the high frequency illuminations produced by the ELS (Figure 19(a)), we can see that the separation results using the high frequency filters are competitive but there is more noise, for example, in the two fluorescent flowers. The decreased amount of light going through the filters likely caused the camera to exhibit more noise. The ratio α/β for the high frequency filters is also much larger than for the spectra produced by the ELS, which makes the separation results more sensitive to the noise from the camera and also contributes to the noise.

5.5 Ambient Illumination

So far, we have extended our method to more general light sources by using high frequency filters instead of the ELS, but we did not consider ambient light. In the following, we discuss the affect that ambient light has on our approach. Let us denote an ambient illuminant as $l_a(\lambda)$. Without loss of generality, the two illuminants produced by either the ELS or flat light source with filters are defined as $l_1(\lambda)$ and $l_2(\lambda)$. So the illuminations with ambient light can be described as

$$\begin{aligned} l_1^a(\lambda) &= l_1(\lambda) + l_a(\lambda), \\ l_2^a(\lambda) &= l_2(\lambda) + l_a(\lambda). \end{aligned} \tag{23}$$

Replacing the $l_n(\lambda)$ by $l_n^a(\lambda)$ in Equation (7), we obtain

$$\begin{aligned} p_1(\lambda) &= [l_1(\lambda) + l_a(\lambda)]r(\lambda) + k_1 e(\lambda), \\ p_2(\lambda) &= [l_2(\lambda) + l_a(\lambda)]r(\lambda) + k_2 e(\lambda), \\ k_n &= \int [l_n(\lambda) + l_a(\lambda)]a(\lambda^{'})\mathrm{d}\lambda^{'}. \end{aligned} \tag{24}$$

Since the ambient illuminant l_a is the same under the two different high frequency illuminants $l_1^a(\lambda)$ and $l_2^a(\lambda)$, the difference between k_1 and k_2 is only related to the high frequency illuminants $l_1(\lambda)$ and $l_2(\lambda)$. Intuitively, the intensity of the ambient illuminant can be considered

This article has been accepted for publication in a future issue of this journal, but has not been fully edited. Content may change prior to final publication. Citation information: DOI 10.1109/TPAMI.2015.2473839, IEEE Transactions on Pattern Analysis and Machine Intelligence

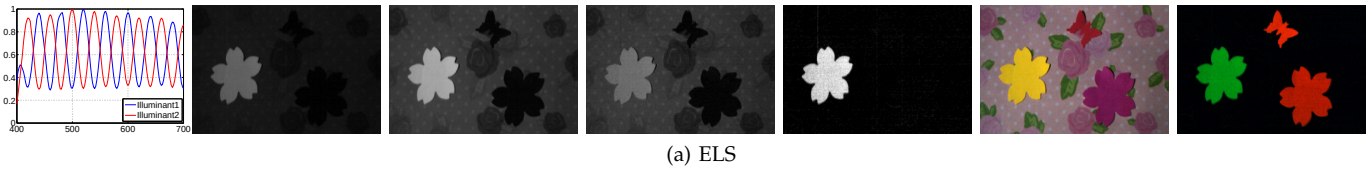

(a) ELS

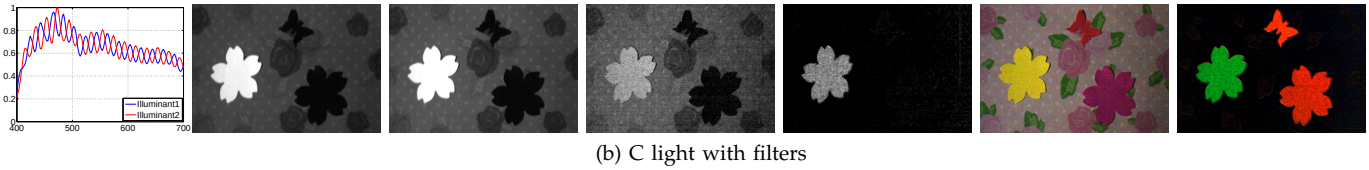

(b) C light with filters

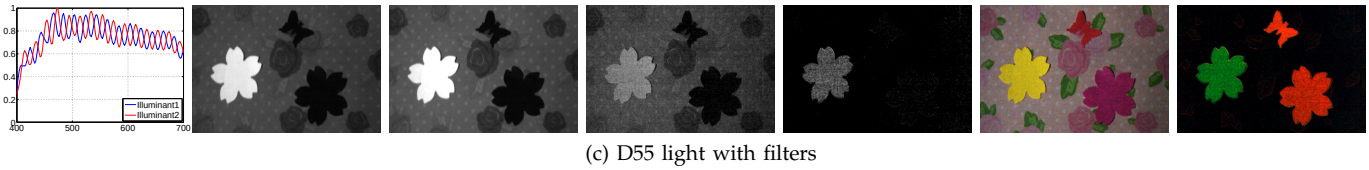

(c) D55 light with filters

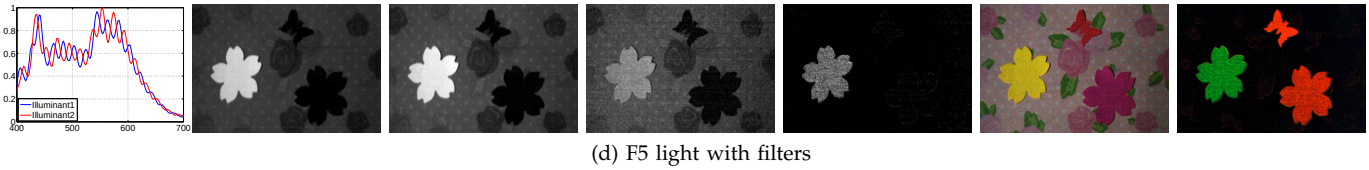

(d) F5 light with filters

Fig. 19: The separation results with the high frequency filters. The spectra of the illuminants are shown in the first column. Taking a channel at 550 nm as an example, the second and third columns show the captured images under 2 high frequency illuminations, and their separated reflective and fluorescent components are shown in third and fourth columns. The fifth and sixth columns show reflective and fluorescent components over all captured spectra in RGB images. To make comparison, the first row shows the separation results under high frequency illuminations produced by ELS. From second to fourth rows, the separation results under C, D55 and F5 lights with the high frequency filters are shown, respectively.

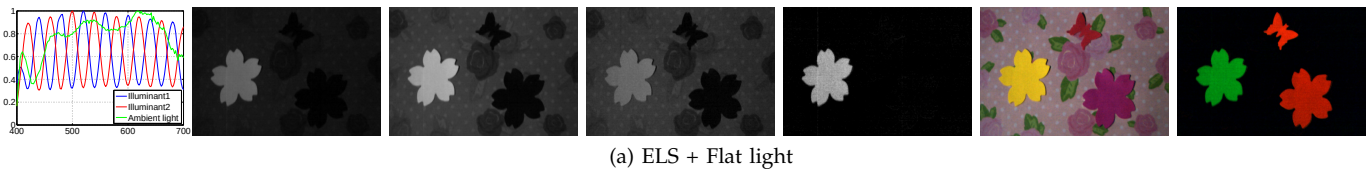

(a) ELS + Flat light

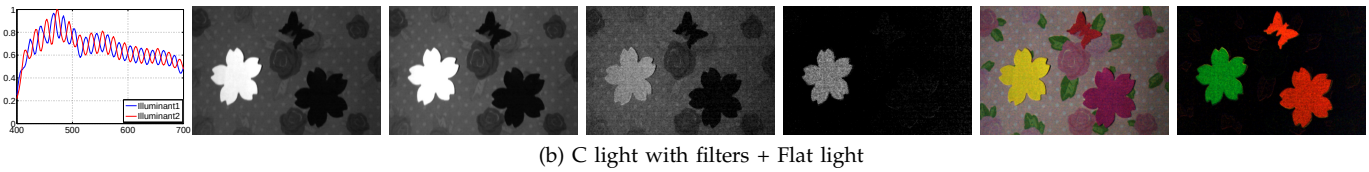

(b) C light with filters + Flat light

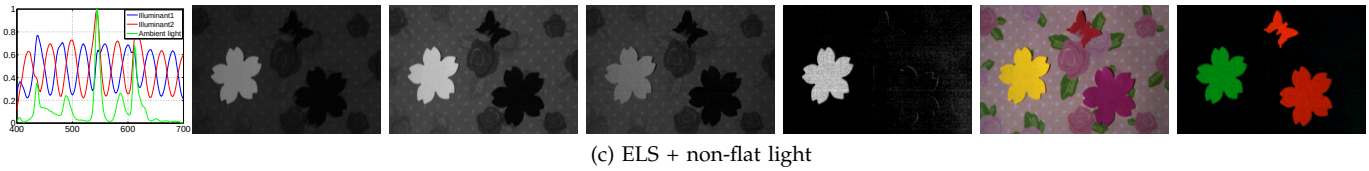

(c) ELS + non-flat light

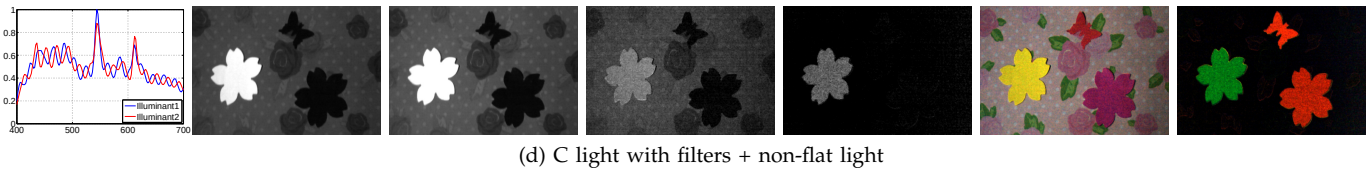

(d) C light with filters + non-flat light

Fig. 20: The separation results with ambient light. The spectra of illuminants are shown in the first column, where the green curves in the first and third rows are the spectra of the flat and non-flat ambient light. Taking a channel at 550 nm as an example, the second and third columns show the captured images under 2 high frequency illuminations, and their separated reflective and fluorescent components are shown in third and fourth columns. The fifth and sixth columns show reflective and fluorescent components over all captured spectra in RGB images. From the first to fourth rows, we see separation results under high frequency illuminants produced by the ELS with flat ambient light (D50), C light through high frequency filters with flat ambient light, high frequency illuminants produced by the ELS with non-flat ambient light (typical of a fluorescent lamp), and C light through high frequency filters with non-flat ambient light, respectively.

This article has been accepted for publication in a future issue of this journal, but has not been fully edited. Content may change prior to final publication. Citation information: DOI 10.1109/TPAMI.2015.2473839, IEEE Transactions on Pattern Analysis and Machine Intelligence

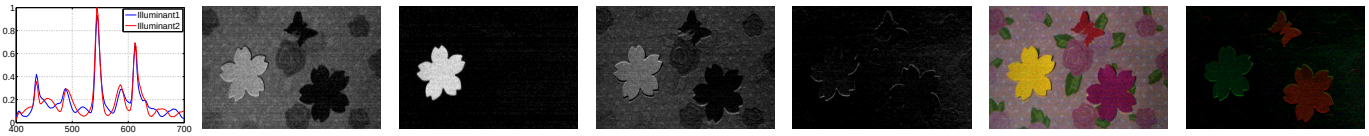

(a) Illuminations (b) p_r (c) p_f (d) p_r (e) p_f (f) p_r (g) p_f

Fig. 21: The separation results under strong ambient light, which is typical of fluorescent lamps. (a) shows the two illuminations used to illuminate scene. (b) and (c) show separation results at crests of the ambient light spectrum at 520 nm, (d) and (e) show results at peaks of the ambient light spectrum 540 nm, and (f) and (g) show results over the visible spectrum as RGB images.

as a part of the DC component α, which is also the same under two complementary high frequency illuminations. Thus, our method can be directly used on scenes with ambient light, and the reflectance and fluorescence emission spectra can be recovered by Equation (8), in which the illuminations $l_n(\lambda)$ are replaced by $l_n^a(\lambda)$.

Figure 20 shows the separation results under different high frequency illuminants and ambient light. The spectra of flat and non-flat ambient lights are shown as green lines in the first column of Figure 20(a) and (c). We can see that all separation results under flat ambient light (Figure 20(a) and (b)) and non-flat ambient light (Figure 20(c) and (d)) are clear. These results demonstrate that our method works well under both flat and non-flat ambient light sources. Compared with the results under the high frequency illuminations produced by the ELS (Figure 20(a) and (c)), the separation results under lights through the high frequency filters (Figure 20(b) and (d)) contain noise like in Figure 19, but are also acceptable.

We also capture the scene under a strong ambient illuminant which is typical of a fluorescent lamp, and show the separation results in Figure 21. The results on the crest located at 520 nm of the ambient light spectrum show clear separation of the components (Figure 20(b) and (c)), while the results on the peak at 540 nm of the ambient light spectrum are clearly wrong (Figure 20(d) and (e)). This is because the DC component in the $l_n^a(\lambda)$ is larger and the observation of two high frequency illuminations will be almost same under the strong ambient illuminant spectrum in that range. The separation results are easily affected by camera noise. Therefore, we need to choose a higher intensity light source when the ambient illuminant is strong in practice.

6 Limitations and Conclusion

In this paper, we presented a method to simultaneously recover the reflectance and fluorescence emission spectra of an entire scene by using high frequency illumination in the spectral domain. Afterward, we presented our method for estimating the fluorescence absorption spectrum of a material given its emission spectrum. Through our method, we also showed that similar emission spectra tend to map to similar absorption spectra. The effectiveness of the proposed method was successfully demonstrated with experiments using real data taken by a spectroradiometer and camera, both in conjunction with a programmable light source. To extend our method to much more general light sources, we designed two high frequency filters and employed them under CIE standard illuminants. We demonstrated that when the light source is flat enough compared with the frequency of the filters, our method also works well. We also implemented our method under high frequency illuminations with flat/non-flat ambient light, and the results show that our method works well under different types of ambient light.

There are still a few limitations in our research that are worth attention and further investigation. First, the two high frequency filters used in our experiments affect the separation results, due to their distortions of the sinusoidal patterns and the differences between the peaks and crests of the light spectra. In the future, we will design/employ much better high frequency filters, which have much smaller distortions, and especially smaller values of α/β, to make them more robust to noise. Second, we did not consider shading from the light source and specularity from the materials in our work. More importantly, shading and specularity can provide more information about a scene. Therefore, it is worth investigating a more comprehensive model for reflective and fluorescent separation to make it applicable to more real cases.

References

[1] C. Balas, V. Papadakis, N. Papadakis, A. Papadakis, E. Vazgiouraki, and G. Themelis, "A novel hyper-spectral imaging apparatus for the non-destructive analysis of objects of artistic and historic value," *J. Cult. Herit.*, vol. 4, no. 1, 2003.

[2] I. B. Styles, A. Calcagni, E. Claridge, F. Orihuela-Espina, and J. M. Gibson, "Quantitative analysis of multi-spectral fundus images." *Medical Image Analysis*, vol. 10, no. 4, 2006.

[3] G. Johnson and M. Fairchild, "Full-spectral color calculations in realistic image synthesis," *IEEE Computer Graphics and Applications*, vol. 19, Aug. 1999.

[4] C. Chi, H. Yoo, and M. Ben-Ezra, "Multi-spectral imaging by optimized wide band illumination," *IJCV*, vol. 86, no. 2-3, Jan. 2010.

[5] J. M. DiCarlo, F. Xiao, and B. A. Wandell, "Illuminating illumination," in *CIC*. IS&T/SID, 2001.

[6] L. T. Maloney and B. A. Wandell, "Color constancy: a method for recovering surface spectral reflectance," *JOSA A*, vol. 3, no. 1, 1986.

[7] S. Tominaga, "Multichannel vision system for estimating surface and illumination functions," *JOSA A*, vol. 13, no. 11, Nov 1996.

[8] N. Gat, "Imaging spectroscopy using tunable filters: A review," in *Wavelet Applications VII*, vol. 4056. SPIE, 2000.

[9] J. Park, M. Lee, M. D. Grossberg, and S. K. Nayar, "Multispectral Imaging Using Multiplexed Illumination," in *ICCV*. IEEE, Oct 2007.

[10] K. Barnard, "Color constancy with fluorescent surfaces," in *CIC,Proceedinds of the IS&T/SID Color Imaging Conference*, 1999.

[11] C. Zhang and I. Sato, "Separating reflective and fluorescent components of an image," in *IEEE Conference on Computer Vision and Pattern Recognition (CVPR)*, 2011.
[12] F. W. D. Rost, *Fluorescence Microscopy*. Cambridge University Press, 1992.
[13] D. A. Skoog, F. J. Holler, and S. R. Crouch, *Principles of Instrumental Analysis*. Thomson Publishers, 2007.
[14] Y. Fu, A. Lam, I. Sato, T. Okabe, and Y. Sato, "Separating reflective and fluorescent components using high frequency illumination in the spectral domain," in *Proc. of International Conference on Computer Vision (ICCV)*, 2013, pp. 457–464.
[15] G. McNamara, A. Gupta, J. Reynaert, T. D. Coates, and C. Boswell, "Spectral imaging microscopy web sites and data," *Cytometry. Part A: the journal of the International Society for Analytical Cytology*, vol. 69, no. 8, 2006.
[16] A. Wilkie, A. Weidlich, C. Larboulette, and W. Purgathofer, "A reflectance model for diffuse fluorescent surfaces," in *International conference on Computer graphics and interactive techniques*, 2006.
[17] M. B. Hullin, J. Hanika, B. Ajdin, H.-P. Seidel, J. Kautz, and H. P. A. Lensch, "Acquisition and analysis of bispectral bidirectional reflectance and reradiation distribution functions," *ACM Trans. Graph.*, vol. 29, 2010.
[18] I. Sato, T. Okabe, and Y. Sato, "Bispectral photometric stereo based on fluorescence," in *Color Imaging Conference: Color Science, Systems, and Applications*, 2012.
[19] T. Treibitz, Z. Murez, B. G. Mitchell, and D. Kriegman, "Shape from fluorescence," in *European conference on Computer Vision*, 2012.
[20] B.-K. Lee, F.-C. Shen, and C.-Y. Chen, "Spectral estimation and color appearance prediction of fluorescent materials," *Optical Engineering*, vol. 40, 2001.
[21] M. Alterman, Y. Schechner, and A. Weiss, "Multiplexed fluorescence unmixing," in *IEEE International Conference on Computational Photography (ICCP)*, 2010.
[22] S. Tominaga, T. Horiuchi, and T. Kamiyama, "Spectral estimation of fluorescent objects using visible lights and an imaging device," in *Proceedinds of the IS&T/SID Color Imaging Conference*, 2011.
[23] A. Lam and I. Sato, "Spectral modeling and relighting of reflective-fluorescent scenes," in *IEEE Conference on Computer Vision and Pattern Recognition (CVPR)*, 2013.
[24] J. Suo, L. Bian, F. Chen, and Q. Dai, "Bispectral coding: compressive and high-quality acquisition of fluorescence and reflectance," *Optics Express*, vol. 22, no. 2, pp. 1697–1712, Jan. 2014.
[25] A. Springsteen, "Introduction to measurement of color of fluorescent materials," *Analytica Chimica Acta*, vol. 380, 1999.
[26] Y. Zheng, I. Sato, and Y. Sato, "Spectra estimation of fluorescent and reflective scenes by using ordinary illuminants," in *Proc. of European Conference on Computer Vision (ECCV)*, 2014, pp. 188–202.
[27] Y. Fu, A. Lam, Y. Kobashi, I. Sato, T. Okabe, and Y. Sato, "Reflectance and fluorescent spectra recovery based on fluorescent chromaticity invariance under varying illumination," in *Proc. of IEEE Conference on Computer Vision and Pattern Recognition (CVPR)*, Jun. 2014, pp. 2171–2178.
[28] H. Farid and E. Adelson, "Separating reflections and lighting using independent components analysis," in *Computer Vision and Pattern Recognition (CVPR)*, Fort Collins, CO, 1999.
[29] S. Nayar, X. Fang, and T. Boult, "Removal of Specularities using Color and Polarization," in *IEEE Conference on Computer Vision and Pattern Recognition (CVPR)*, Jun 1993.
[30] S. K. Nayar, G. Krishnan, M. D. Grossberg, and R. Raskar, "Fast separation of direct and global components of a scene using high frequency illumination," *ACM Trans. Graph.*, vol. 24, no. 3, Jul. 2006.
[31] C. Zhang and I. Sato, "Image-based separation of reflective and fluorescent components using illumination variant and invariant color," *IEEE Transactions on Pattern Analysis and Machine Intelligence*, vol. 35, no. 12, pp. 2866–2877, Dec. 2013.
[32] A. V. Oppenheim, A. S. Willsky, and w. S. Hamid, *Signals and Systems*, 2nd ed. Prentice Hall, Aug. 1996.
[33] D. Donoho, Y. Tsaig, I. Drori, and J.-L. Starck, "Sparse solution of underdetermined systems of linear equations by stagewise orthogonal matching pursuit," *IEEE Transactions on Information Theory*, vol. 58, no. 2, 2012.
[34] E. Candes and T. Tao, "Near-optimal signal recovery from random projections: Universal encoding strategies?" *IEEE Transactions on Information Theory*, vol. 52, no. 12, 2006.
[35] B. Efron, T. Hastie, I. Johnstone, and R. Tibshirani, "Least angle regression," *Annals of Statistics*, vol. 32, 2004.
[36] R. W. G. Hunt and M. R. Pointer, *Measuring Colour*, 4th ed. John Wiley & Sons, Ltd, Sep. 2011.

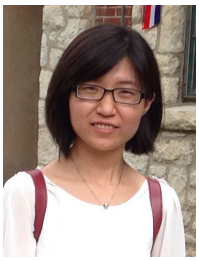

Ying Fu received the B.S. degree in Electronic Engineering from Xidian University in 2009 and the M.S. degree in Automation from Tsinghua University in 2012. She joined the graduate school of information science and technology at the University of Tokyo in 2012, where she is currently a Ph.D. candidate under the supervision of Prof. Yoichi Sato. Her research interests include physics-based vision, image processing, and computational photography.

Antony Lam received the B.S. degree in Computer Science at the California State Polytechnic University, Pomona in 2004 and the Ph.D. in Computer Science at the University of California, Riverside in 2010. After working at the National Institute of Informatics, Japan, he joined the Graduate School of Science and Engineering at Saitama University as an assistant professor in 2014. His research interests are mainly in computer vision with emphasis on the areas of physics-based vision and pattern recognition.

Imari Sato received the B.S. degree in policy management from Keio University in 1994. After studying at the Robotics Institute of Carnegie Mellon University as a visiting scholar, she received the M.S. and Ph.D. degrees in interdisciplinary Information Studies from the University of Tokyo in 2002 and 2005, respectively. In 2005, she joined the National Institute of Informatics, where she is currently an associate professor. Her primary research interests are in the fields of computer vision (physics-based vision, image-based modeling) and Computer Graphics (image-based rendering, augmented reality). She has received various research awards, including IPSJ Nagao Special Researcher award (2010), The Young Scientists' Prize from The Commendation for Science and Technology by the Minister of Education, Culture, Sports, Science and Technology (2009), and Microsoft Research Japan New Faculty award (2011).

Takahiro Okabe received the B.S. and M.S. degrees in physics, and the Ph.D. degree in information science and technology from the University of Tokyo, Japan, in 1997, 1999 and 2011 respectively. After working at the Institute of Industrial Science, the University of Tokyo, he joined Kyushu Institute of Technology, Japan, as an associate professor in 2013. His research interests include computer vision, image processing, pattern recognition, and computer graphics, in particular their physical and mathematical aspects.

Yoichi Sato is a professor at Institute of Industrial Science, the University of Tokyo. He received his B.S. degree from the University of Tokyo in 1990, and his M.S. and Ph.D. degrees in robotics from School of Computer Science, Carnegie Mellon University in 1993 and 1997 respectively. His research interests include physics-based vision, reflectance analysis, image-based modeling and rendering, and gaze and gesture analysis. He served/is serving in several conference organization and journal editorial roles including IEEE Transactions on Pattern Analysis and Machine Intelligence, International Journal of Computer Vision, Computer Vision and Image Understanding, IET Computer Vision, IPSJ Journal of Computer Vision and Applications, ECCV2012 Program Co-Chair and MVA2013 General Chair.